# ARTI: One New Adaptive Elliptical Weighting Model Combining with the Tikhonov-$\ell_p$-norm for Image Reconstruction

Chunhua Zhu[1,2,3(✉)], Zhen Shi[1,2,3], and Weidong Yang[1,2,3]

[1] Key Laboratory of Grain Information Processing and Control, Ministry of Education, Henan University of Technology, Zhengzhou 450001, Henan, China
zhuchunhua@haut.edu.cn
[2] College of Information Science and Engineering, Henan University of Technology, Zhengzhou 450001, Henan, China
[3] Henan Key Laboratory of Grain Photoelectric Detection and Control, Henan University of Technology, Zhengzhou 450001, Henan, China

**Abstract.** To reconstruct the target-induced attenuation image keeping consistent with the observed measurement data, this paper explores the use of a new horizontal distance attenuation-based elliptical weighting model in building an attenuation image, where a horizontal distance attenuation factor and a vertical distance attenuation factor are introduced, respectively, which is able to clear the difference of the voxel weightings perpendicular to the line-of-sight (LOS) direction, as well as the difference of the voxel weightings parallel to the LOS direction. Compared with the existing model, the proposed model can additively reflect the occlusion effect of the radio frequency signal when the target is close to the transceiver nodes. Besides, the Tikhonov-$\ell_p$-norm regularization is incorporated into the image reconstruction, which makes full use of the sparse ability of the $\ell_p$-norm ($0 < p < 1$) to further reduce the noise interference. The experimental studies on indoor and outdoor scenarios with radio tomographic imaging are presented to validate the effectiveness of the proposed approach.

**Keywords:** Device-free localization · Radio tomographic imaging · Elliptical weighting model · $\ell_p$-norm · Horizontal distance attenuation

## 1 Introduction

Radio tomographic imaging (RTI) technology can image the received signal strength (RSS) changes of wireless propagation within the wireless sensor networks (WSNs) area, where several mathematical models are applied to reconstruct images of moving targets in indoor and outdoor environments with low power and low cost [1]. In an RTI system, the elliptical weighting model has obtained widely application to derive the shadowing losses on links between many pairs of nodes in a wireless network, then image the attenuation of targets. The classical weighting model [2] was first proposed by Joey Wilson and Neal Patwari, which builds one ellipse by taking any two transceiver nodes as the elliptical focus; the voxel weightings within the ellipse are all equal


W. Xiang et al. (Eds.): BROADNETS 2021, LNICST 413, pp. 208–225, 2022.
https://doi.org/10.1007/978-3-030-93479-8_14

to one, and zero for the others, that is, the voxel weightings within the ellipse can't be distinguished. In 2014, Benjamin R. Hamilton proposed the inverse area elliptical model [3], which modeled the weight of each voxel as the reciprocal of the minimum ellipse area containing two sensor nodes and the voxel. The proposed model is able to distinguish the contribution of each voxel in the ellipse, and obtain greater positioning accuracy than other models. However, the higher computational complexity makes it impossible to apply in real time. In 2015, a const-eccentricity elliptical model was proposed in [4]. In the proposed model, the minor axis parameters of ellipse are positively correlated with link length, and images can be reconstructed with fewer voxels, thus noise interference is greatly reduced. But, how to determine the weightings inside the ellipse has not been considered. In 2019, an adaptive elliptical weighting model considering both the adjustment of ellipse coverage and the selection of voxel weighting was proposed in [6], and the indoor positioning and tracking experiments verify that the model can improve RTI performance. Besides, there are other elliptical models based on Fresnel diffraction theory, such as saddle surface model [12] and diffraction model [13, 14]. However, these models no longer define voxel weightings, but concern RSS changes, which can't be directly applied to the existing RTI systems.

Reviewing the existing research, for improving the image reconstruction quality and the positioning accuracy, the voxel weightings in one ellipse should be chosen to match the actual attenuation of the measurement data, besides, adjusting the range of the ellipse and selecting the optimal image reconstruction algorithm can deduce the interference of reconstructed images. In this paper, an innovative elliptical model is presented, which introduces an adaptive horizontal distance attenuation factor based on the adaptive elliptical model [6], so that the voxel weightings become a function of the horizontal distance and the vertical distance between the voxel and the transceiver nodes, thereby the new elliptical weighting model is able to better match the measurements.

Besides, a Tikhonov-$\ell_p$-norm regularization is proposed to solve the ill-posed linear equations for imaging target position. The Tikhonov regularization is usually applied to transform the ill-posed problems into well-posed optimization problems [24], the target position can be estimated from Tikhonov regularized solution, but which is smoother resulting in inaccurate positioning. Actually, the target only occupies a few voxels in the whole monitoring area, which satisfies the sparsity of structure. Moreover, the compressive sensing (CS)-based solutions, such as the least absolute shrinkage and selection operator (LASSO) [25] and orthogonal matching pursuit (OMP) [5, 16], have been proven. However, compared with CS-based image reconstruction, Tikhonov regularized solution [17] can provide higher positioning accuracy. In 2019, Xu [7] proposed a novel regularized reconstruction method (referred to as Tikhonov-$\ell_1$-norm regularization) with the objective function of linearly combining $\ell_1$-norm and $\ell_2$-norm regularization, which utilizes the correlation and sparsity of attenuated images, therefore improves the positioning accuracy and maintains the better imaging quality.

In fact, the optimization model under $\ell_1$-norm sparse constraint needs more observation data to ensure the positioning accuracy in practical application, and there are several non-convex reconstruction models are proved to perform better than the $\ell_1$-norm at low sampling rate [26], such as $\ell_0$-norm and $\ell_p$-norm. However, $\ell_0$-norm-based optimization model is a mathematical non-deterministic polynomial (NP) problem.

Instead, $\ell_p$-norm ($0 < p < 1$) [23] can also promote the sparsity of the solution and avoid making the regular solution smoother. In this paper, the Tikhonov-$\ell_p$-norm regularization will be explored in detail for image reconstruction in RTI system.

This paper is organized as follows: in Sect. 2, the principle of RTI and the proposed adaptive elliptical model are introduced. The $\ell_p$-norm-based reconstruction method is presented in Sect. 3. The experiments in indoor and outdoor scenarios are given and analyzed in Sect. 4. Finally, the conclusion is presented in Sect. 5.

## 2 Radio Tomographic Imaging

### 2.1 Introduction of RTI

As illustrated in Fig. 1, there are $L$ sensor nodes deployed around the monitor area, and the red ellipse represents the target. A communication link or LOS path is established between any two sensor nodes, and the total number of links can be denoted as $M = L(L-1)$. The monitor area is divided into $N$ grids (referred to as voxels). When a target enters the monitor area, the RSS value will be changed as [8, 15]

$$\mathbf{y} = \mathbf{W}\mathbf{x} + \mathbf{n} \tag{1}$$

where $\mathbf{y} = [y_1, y_2, \ldots, y_M]^T \in \mathbf{R}^M$ denotes the RSS changes of all the links in the network, $\mathbf{W} = [\mathbf{w}_1, \mathbf{w}_2, \ldots, \mathbf{w}_M]^T \in \mathbf{R}^{M \times N}$ means the shadow weight matrix, $\mathbf{w}_i = [w_{i,1}, w_{i,2}, \ldots, w_{i,N}] \in \mathbf{R}^N$, $\mathbf{x} = [x_1, x_2, \ldots, x_N]^T \in \mathbf{R}^N$ is the signal fading value in the voxel, $\mathbf{n} = [n_1, n_2, \ldots, n_M]^T \in \mathbf{R}^M$ is the measurement noise vector.

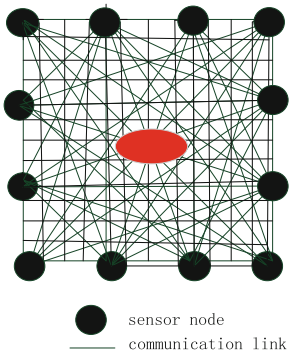


**Fig. 1.** RTI sensor node deployment.

When reconstructing a target image from measurement data, it needs to search for an optimal solution under the least-squared (LS) error:

$$\mathbf{x}_{LS} = \arg\min_{\mathbf{x}} \|\mathbf{W}\mathbf{x} - \mathbf{y}\|_2^2 \tag{2}$$

In RTI system, $\mathbf{W}$ is not full-rank, therefore, the LS solution of Eq. (2) will not be unique. In the classical RTI, the prior information of the attenuation signal $\mathbf{x}$ is added to the solution process as a constraint term, and the attenuation image can be reconstructed by Tikhonov regularization, the corresponding objective function is expressed as:

$$\min f(\mathbf{x}) = \|\mathbf{W}\mathbf{x} - \mathbf{y}\|_2^2 + \mu_1 \mathbf{x}^T \mathbf{C}^{-1} \mathbf{x} \tag{3}$$

where $\mu_1$ is the Tikhonov regularization parameter [10]. $\mathbf{C}$ is the prior covariance matrix of $\mathbf{x}$, which can be approximately calculated as

$$[\mathbf{C}]_{lj} \approx \exp(-\frac{d_{lj}}{\delta}) \tag{4}$$

where $d_{lj}$ is the distance from voxel $l$ to voxel $j$, and $\delta$ is a "space constant" correlation parameter [1].

Setting the gradient of Eq. (3) to zero, the solution of Tikhonov regularization can be obtained:

$$\tilde{\mathbf{x}} = (\mathbf{W}^T\mathbf{W} + \mu_1 \mathbf{C}^{-1})^{-1} \mathbf{W}^T \mathbf{y} \tag{5}$$

here the target location is the voxels with the largest attenuation in the reconstructed image $\tilde{\mathbf{x}}$.

### 2.2 Elliptical Weighting Model Considering Horizontal Distance Attenuation

The weighting model can decide whether a voxel contributes to image reconstruction. Figure 2 shows the elliptical weighting model in the RTI system, where any two sensor nodes can be the foci of the ellipse, as Fig. 2(a) for the longest link.

In the classical weighting model [2] (referred to as Model 1), the parameter $\lambda$ for adjusting the minor axis length of ellipse is a constant, which is obtained by experiments or estimated on-line [11]. If the voxel is within the ellipse, its weight is set to 1; otherwise, the weight is set to 0. In addition, as shown in link1 and link2 in Fig. 2(b), the link lengths may be different. Therefore, considering the influence of the link length on the weight, the weight inside the ellipse needs to be multiplied by the reciprocal of the square root of the link length:

$$w_{i,j} = \frac{1}{\sqrt{d_i}} \begin{cases} 1 & d_{ij}(1) + d_{ij}(2) < d_i + \lambda \\ 0 & otherwise \end{cases} \tag{6}$$

where $d_i$ is the length of link $i$, and $d_{ij}(1)$, $d_{ij}(2)$ are the distances between voxel $j$ and two sensor nodes, respectively.

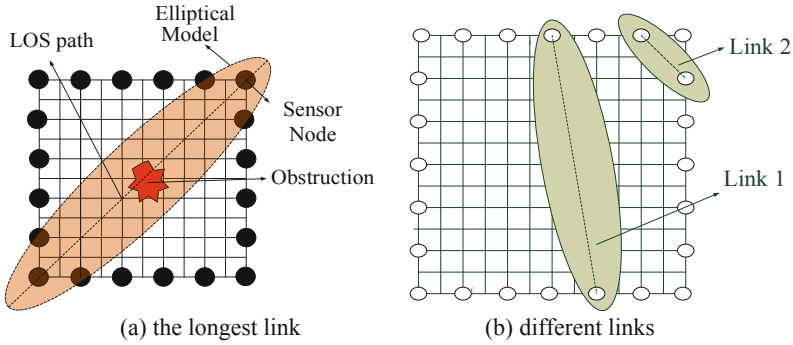


**Fig. 2.** The elliptical weighting model.

According to Eq. (6), $\lambda$ is a fixed value for different $d_i$. Thereby, the shorter link length will lead to the bigger elliptical coverage which will introduce more measurement noise.

To solve the above problem, the const-eccentricity weight model (referred to as Model 2) is proposed in [4], which can be described as

$$w_{i,j} = \frac{1}{\sqrt{d_i}} \begin{cases} 1 & d_{ij}(1) + d_{ij}(2) < d_i + \frac{d_i}{d\max}\lambda \\ 0 & otherwise \end{cases} \tag{7}$$

where $d_{\max}$ corresponds to the length of the longest link.

However, for Model 1 and Model 2, the attenuation contributions of different voxels in the same ellipse can't be distinguished, which leads to the mismatching between the weigh model and the measured data. For improving the positioning performance, an adaptive elliptical weight model (referred to as Model 3) is proposed in [6], which introduces one distance attenuation factor $e^{-h}$ and the adaptive weighing value is defined as

$$w_{i,j} = \begin{cases} e^{-h} & d_{ij}(1) + d_{ij}(2) < d_i + \varphi\lambda \\ 0 & otherwise \end{cases} \tag{8}$$

where $e$ is the base of the natural logarithm and $h$ is the vertical distance from voxel $j$ to the LOS path, and $\varphi$ is a parameter adjusting the minor axis of ellipse adaptively:

$$\varphi = \frac{d_{\max}}{d_i} \tag{9}$$

According to Eq. (8), the weightings of voxels will change inversely with parameter $h$. For the shorter link, the coverage of the corresponding ellipse will become larger, and there is more valid measurement information for the following image reconstruction.

In fact, according to the attenuation characteristics of radio propagation, the voxel weight is not only related to the vertical distance from the voxel to the LOS path, but also related to the horizontal distance from the voxel to any two sensor nodes. The closer the voxel is to the sensor node, the greater the occlusion effect is on the node. Therefore, we can define the greater voxel weight to match the more RSS attenuation. Combined with the prior information **x**, that is, the distribution of the attenuation map accords with the Gaussian process [18, 19], the horizontal and vertical distance attenuation factors can be expressed as exponential form, which are introduced into the proposed ellipse model (referred to as Model 4):

$$w_{i,j} = \begin{cases} e^{-h} * e^{-s} & d_{ij}(1) + d_{ij}(2) < d_i + \varphi\lambda \\ 0 & otherwise \end{cases} \tag{10}$$

where $s$ is the normalized distance between the projection point of voxel $j$ on the LOS path and any two sensor nodes.

$$\begin{aligned} s &= \min(l_1, l_2)/d_i \\ d_i &= l_1 + l_2 \end{aligned} \tag{11}$$

where $l_1$ and $l_2$ are the distances between the projection point of voxel $j$ on the LOS path and two sensor nodes, respectively, as shown in Fig. 3.

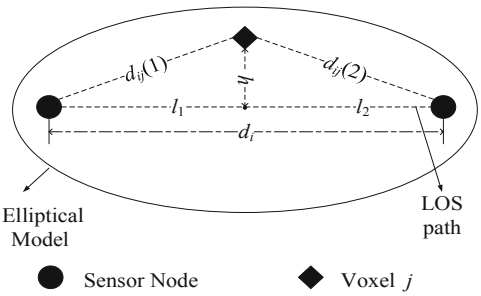


**Fig. 3.** Geometry of elliptical weighting model.

According to Eq. (10), our proposed model mainly includes two characteristics. Firstly, for the pixels in any two ellipses with different coverages, the corresponding pixel weighting can be distinguished despite of the same $\min(l_1, l_2)$ and $h$; secondly, for the pixels in one ellipse, those contribution reflecting path attenuation can be detailed to match the actual radio propagation.

Under the same link, the voxel weighting distribution of different ellipse model are shown in Fig. 4(a), Fig. 4(b), Fig. 4(c), Fig. 4(d), the color bar represents voxel weight, changing from 0–1. It can be seen that the weights of the voxels outside the ellipse are 0. In Fig. 4(a) and Fig. 4(b), the weights of all voxels are constant by Model

1 and Model 2 respectively. The weights of voxels by Model 3 only change in the vertical direction to the LOS path, that is, the weights of voxels are only related to the parameter $h$ as Eq. (8). Besides, compared with Model 1, the other ellipse coverage can change with own adjustment parameters. In Model 4, the weights of voxels have the greater weights for the closer distance from the nodes, including the vertical direction and horizontal direction.

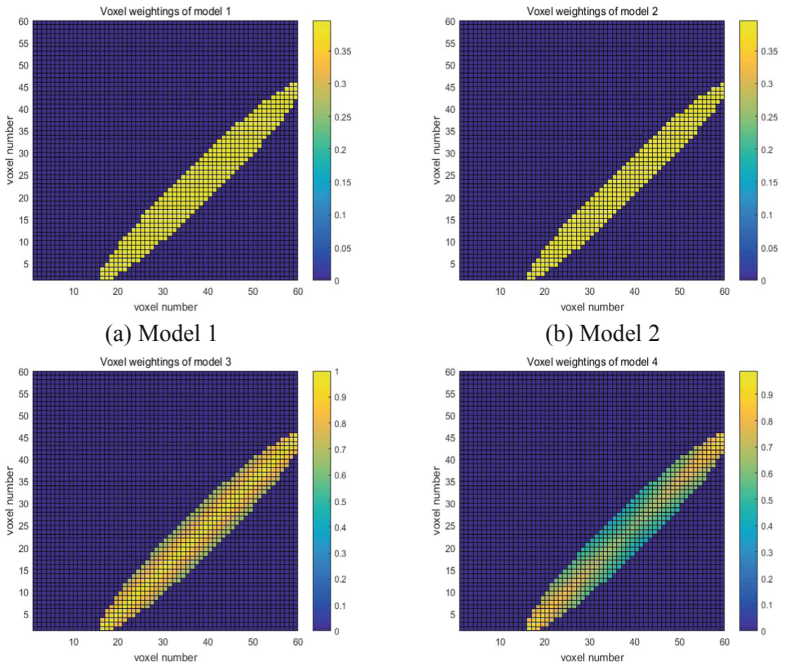


(a) Model 1 (b) Model 2

(c) Model 3 (d) Model 4

**Fig. 4.** Voxel weightings distribution of different elliptical models.

In order to evaluate the matching degree between the weighting model and measured data, the experiment of two WSN nodes is carried out as shown in Fig. 5(a), one target moves from (–1.6, 0) to (1.6, 0) along the LOS path and from (0, –1.1) to (0, 1.1) along the NLOS path as shown in Fig. 5(b). The collected RSS information in X and Y direction are shown, respectively, here the normalized RSS values have been fit to accessible curve. It can be seen that the attenuation trend is symmetrical round the origin of the axes as in Fig. 5(c) and Fig. 5(d), which is the center of link between two nodes, and X coordinate represents the horizontal direction of the communication link, Y coordinate represents the vertical direction of the communication link. From Fig. 5 (c), the RSS attenuation increases steadily when the target moves along LOS path from the center of link towards one node; and in the horizontal direction of the communication link of NLOS path, there is the worse RSS attenuation for the shorter vertical

distance when the target moves near the center of the link. These worse RSS attenuations should correspond to the larger voxel weights, the proposed ellipse model (Model 4) can reflect the above RSS attenuation characteristics in RTI.

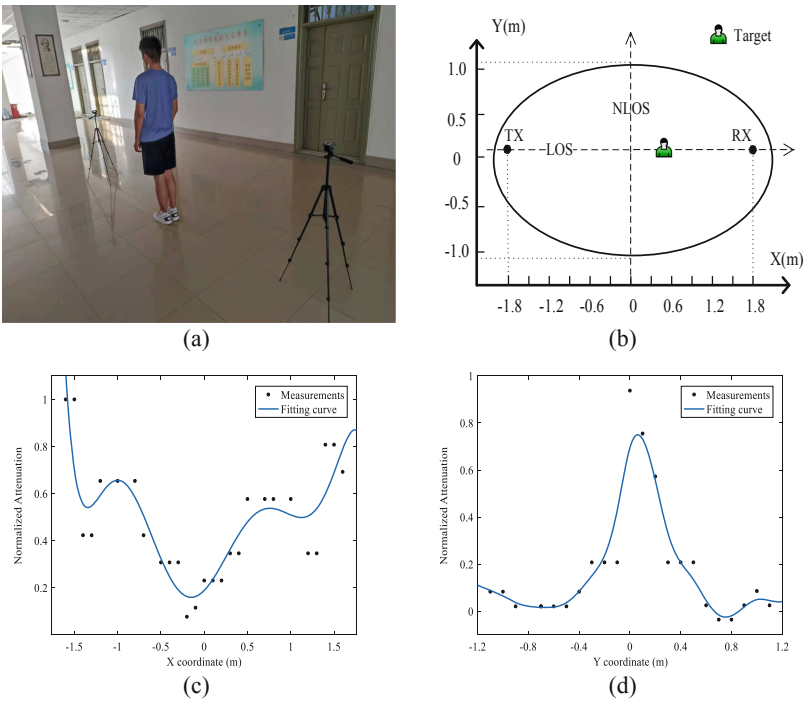


**Fig. 5.** The verification on the RSS attenuation characteristics in RTI. (a) the experiment scenario. (b) Illustration of the experimental setup. (c) RSS attenuation along the LOS path. (d) RSS attenuation along the NLOS path.

## 3 TIKHONOV-$\ell_p$-norm-Based Image Reconstruction

Substituting Eq. (10) into Eq. (5), we can obtain the signal fading value of all voxels $\mathbf{x}$ in the monitoring area, then the Tikhonov regularization can solve the linear equations as Eq. (3) for imaging target position [24, 27, 28]. In several cases, there will inevitably appear artifacts and false targets in the reconstructed image because of the RSS measurement noise and calculation error of fading voxel weightings which will further deteriorate the quality of reconstructed image for the complex scenarios. Considering that the solution of the objective function as Eq. (3) satisfies the sparsity of structure, and combining the correlation among the fading voxels, the $\ell_p$-norm($0 < p < 1$) is

introduced as a sparse constraint to Eq. (3), then the new objective function can be obtained.

$$\min f(\mathbf{x}) = \|\mathbf{W}\mathbf{x} - \mathbf{y}\|^2 + \mu_1 \mathbf{x}^T \mathbf{C}^{-1} \mathbf{x} + \mu_2 \|\mathbf{x}\|_p^p \tag{12}$$

where $\mu_2$ is $\ell_p$-norm regularization parameter.

Sorting Eq. (12), we have

$$\min f(\mathbf{x}) = \mathbf{x}^T (\mathbf{W}^T \mathbf{W} + \mu_1 \mathbf{C}^{-1}) \mathbf{x} - 2\mathbf{x}^T \mathbf{W}^T \mathbf{y} + \mathbf{y}^T \mathbf{y} + \mu_2 \|\mathbf{x}\|_p^p \tag{13}$$

Since $\mathbf{W}^T \mathbf{W} + \mu_1 \mathbf{C}^{-1}$ is positive definite [7], the Cholesky decomposition is

$$\mathbf{W}^T \mathbf{W} + \mu_1 \mathbf{C}^{-1} = \mathbf{Q}^T \mathbf{Q} \tag{14}$$

Plugging Eq. (14) into Eq. (13), the objective function becomes

$$\min f(\mathbf{x}) = \|\mathbf{Q}\mathbf{x} - \mathbf{b}\|^2 + \mu_2 \|\mathbf{x}\|_p^p + \Psi \tag{15}$$

where $\mathbf{b} = (\mathbf{Q}^T)^{-1} \mathbf{W}^T \mathbf{y}$ and $\Psi = \mathbf{y}^T \mathbf{y} - \mathbf{b}^T \mathbf{b}$ are constants independent of $\mathbf{x}$. In this case, Eq. (15) can be transformed into the standard form of $\ell_p$-norm regularization, but which is a non-convex optimization problem. Fortunately, there exist several optimization algorithms based on the $\ell_p$-norm [20–22] for this type of problem.

However, the Tikhonov-$\ell_p$-norm regularization as Eq. (15) isn't the mixed norm [21], and the matrix $\mathbf{Q}$ is full rank, so the optimization algorithms in [20, 21] cannot be directly applied to solve Eq. (15). Considering the complexity of the algorithm, we can mirror the idea of sparse constrained regularization method [22].

Defining the weight coefficient matrix $\mathbf{A}$

$$\begin{aligned} &\mathbf{A} = \mathrm{diag}[a_1, \ldots, a_j, \ldots, a_N] \in \mathbf{R}^{N \times N} \\ &a_j = \left( (x_j^{k-1})^2 + \delta \right)^{-1 + p/2} \end{aligned} \tag{16}$$

where $x_j^{k-1}$ is obtained from the last iteration; $\delta$ is initialized to 1, $k$ is the number of iterations. The solution of the $k$th iteration can be calculated as

$$\mathbf{x}^k = \Omega^k \mathbf{Q}^T (\mathbf{Q} \Omega^k \mathbf{Q}^T + \mu_2 \mathbf{I})^{-1} \mathbf{b} \tag{17}$$

where $\mathbf{I} \in \mathbf{R}^{N \times N}$ is identity matrix, $\Omega^k$ is the diagonal matrix.

$$\Omega^k = diag(1./\mathbf{A}) \tag{18}$$

The detailed iteration process is shown in Algorithm 1.

**Algorithm 1** Iteration Process of Image Reconstruction

**Input:** Matrices $\mathbf{b}$, $\mathbf{Q}$; Parameters $\delta$, $p$, $\mu_2$; Initialize $\mathbf{x}^0 = \mathbf{Q} \setminus \mathbf{b}$, $k = 1$;

**while** $\delta \le 10^{-6}$ **do**

Construct the weight coefficient matrix $\mathbf{A}$ as

**for** $j = 1 : N$

$$a_j = ((x_j^{k-1})^2 + \delta)^{-1+p/2};$$

**end**

$\mathbf{A} = diag[a_1, a_2, ..., a_N]$;

$\mathbf{\Omega}^k = diag(1./\mathbf{A})$;

Update the matrix $\mathbf{x}^k$ as:

$\mathbf{x}^k = \mathbf{\Omega}^k \mathbf{Q}^T (\mathbf{Q}\mathbf{\Omega}^k \mathbf{Q}^T + \mu_2 \mathbf{I})^{-1} \mathbf{b}$;

**if** $||\mathbf{x}^k - \mathbf{x}^{k-1}||^2 \le \sqrt{\delta}/100$ **then**

$\delta = \delta/10$;

**end**

$k = k + 1$;

**end**

**Output:** Reconstructed Shadowing Image $\mathbf{x}^k$

## 4 Experimental Validation and Performance Analysis

### 4.1 Experiment Setup

To verify the effectiveness of the proposed algorithm, several experiments are carried out in outdoor and indoor scenarios as in Fig. 6(a) and Fig. 6(b), respectively, of which the monitoring area is a square of 4.5 m by 4.5 m in Fig. 6(a) and 6 m by 6 m in Fig. 6 (b). The relevant experiment parameters are listed in Table 1. In order to suppress the reflected signal, the flat directional antenna with horizontal beam width of 110° and vertical beam width of 30° are adapted, and the nodes are placed on the bracket with the height of 1m from ground. The nodes fully support the IEEE 802.15.4 protocol, and the maximum transmission power is 4.5 dBm, ensuring to cover the whole monitoring area. In order to measure RSS of all links quickly, a token-ring-like communication protocol [1] was adopted. When all nodes complete a round of signal transmission, RSS measurement information from all links is obtained.


(a) outdoor scenarios (b) indoor scenarios

**Fig. 6.** Experimental scenarios.

**Table 1.** Experiment parameters.

| | Node Spacing | Voxel Size | Node Number | $N$ | $\lambda$ |
|---|---|---|---|---|---|
| Indoor | 1.5 m | 0.1 m × 0.1 m | 16 | 3600 | 0.05 |
| Outdoor | | | 12 | 2025 | 0.04 |

### 4.2 Positioning Performance Evaluation

For evaluating the positioning performance of different ellipse models and reconstruction methods, there are multiple index relevant to the image quality and positioning accuracy is adapted.

Defining the image quality $\sigma_i^2$ of the $i$-th target position is the difference between the normalized reconstructed image $\tilde{\mathbf{x}}_r$ and the true image $\mathbf{x}_i$,

$$\sigma_i^2 = \frac{\left\| \tilde{\mathbf{x}}_r - \mathbf{x}_i^2 \right\|}{N} \tag{19}$$

Here the true image $\mathbf{x}_i$ is modeled as a rectangle of 40 cm by 20 cm:

$$[\mathbf{x}_i]_j = \begin{cases} 1, & \textit{if the target occupies voxel } j \\ 0, & \textit{otherwise} \end{cases} \tag{20}$$

For $N_T$ tested target positions, the average imaging quality and positioning accuracy respectively is:

$$\begin{aligned} RMSE_{(img)} &= \sqrt{\frac{1}{N_T}\sum_{k=1}^{N_T}\sigma_i^2} \\ RMSE_{(loc)} &= \sqrt{\frac{1}{N_T}\sum_{k=1}^{N_T}\left\|\mathrm{z}_k - \tilde{z}_k\right\|^2} \end{aligned} \tag{21}$$

where $\tilde{z}_k$ and $\mathrm{z}_k$ represent the estimated value and real value of the $k$-th target position, respectively.

### 4.3 Performance Analysis of Different Ellipse Models

Assuming three outdoor target positions with (3.0 m, 3.0 m), (2.3 m, 2.3 m) and (1.5 m, 0.9 m), and adapting the Tikhonov reconstruction method, the reconstructed images by Model 1, Model 2, Model 3 and Model 4 respectively are shown as in Fig. 7. The brightest area is the target position, which is the worst attenuation voxel; and the energy concentration degree of the brightest area can embody the positioning performance. It can be seen from Fig. 7 that the proposed Model 4 can show higher energy concentration degree and the less artifact area for different target positions, mainly because of perfect matching between the Model 4 and the actual measured data.

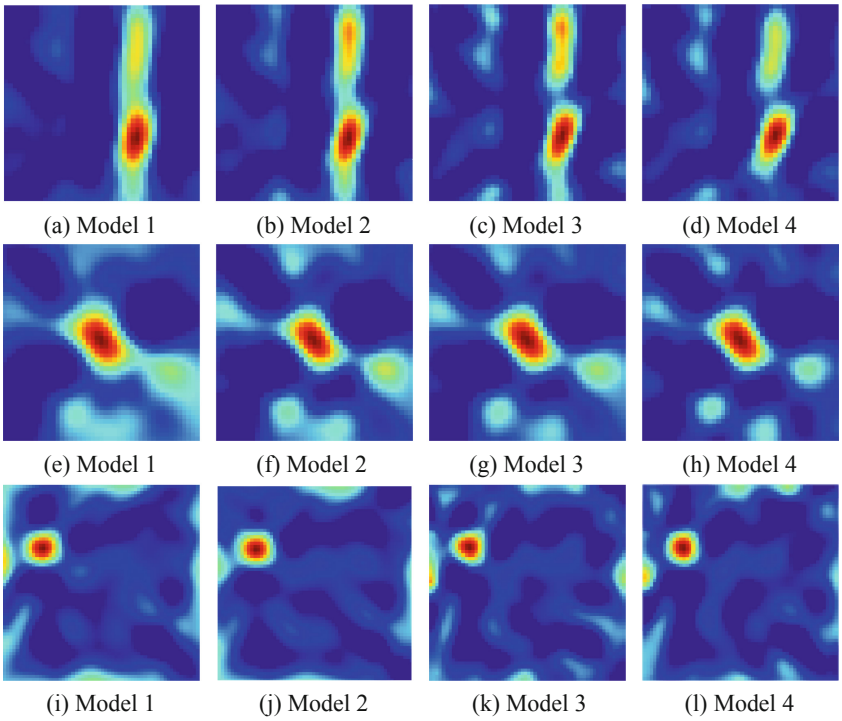


**Fig. 7.** The reconstructed image of different positions in outdoor scenarios. (a)–(d) position 1. (e)–(h) position 2. (i)–(l) position 3

In indoor scenarios, for positions (3.0 m, 4.8 m), (1.0 m, 1.2 m) and (4.8 m, 4.8 m), the reconstructed images are shown in Fig. 8. It can be seen that the positioning performance in indoor scenario is poorer than that in outdoor scenario, mainly rooting from indoor multipath effects.

The imaging quality and positioning error in different target positions also are provided as Fig. 9a and Fig. 9b, which is consistent to the conclusion from Fig. 7 and Fig. 8. The positioning and imaging results are listed in Table 2 lists. Compared with

the other ellipse models, the imaging quality of Model 4 can be improved by about 15.2%, 9.9% and 3.7%, respectively; and the positioning accuracy of Model 4 increases by 31.8%, 19.9% and 9.8%, respectively.

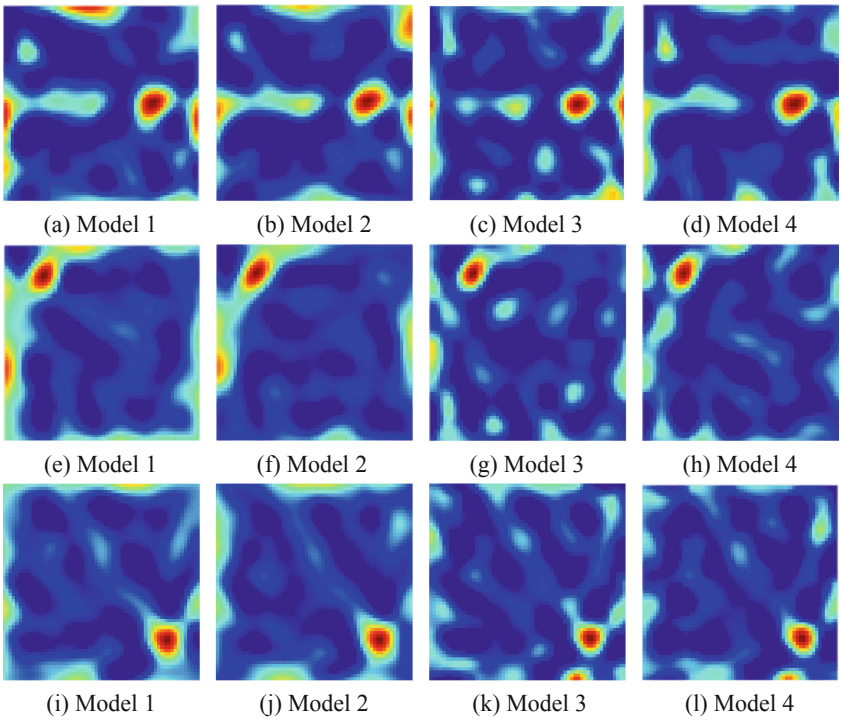


**Fig. 8.** The reconstructed image of different positions in indoor scenarios. (a)–(d) position 4. (e)–(h) position 5. (i)–(l) position 6.

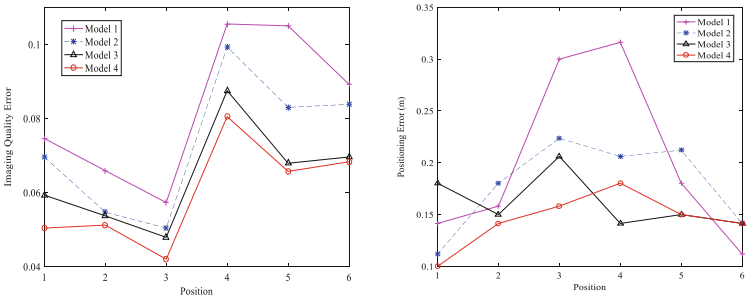


(a) Imaging quality (b) Positioning error

**Fig. 9.** Positioning performance in different target positions.

**Table 2.** Positioning performance of different ellipse models.

| | | Model 1 | Model 2 | Model 3 | Model 4 |
|---|---|---|---|---|---|
| Imaging Quality | $RMSE_{(img)}$ | 0.3154 | 0.2969 | 0.2778 | 0.2676 |
| | Median | 0.2862 | 0.2762 | 0.2522 | 0.2418 |
| | Standard Deviation | 0.0355 | 0.0351 | 0.0272 | 0.0291 |
| Positioning Accuracy (m) | $RMSE_{(loc)}$ | 0.2366 | 0.2013 | 0.1789 | 0.1613 |
| | Median | 0.1696 | 0.1937 | 0.1500 | 0.1458 |
| | Standard Deviation | 0.0859 | 0.0442 | 0.0261 | 0.0264 |

### 4.4 Comparative Analysis of Different Image Reconstruction

The proposed Model 4 is selected as the ellipse model in RTI, and positioning performance of the proposed Tikhonov-$\ell_p$-norm-based image reconstruction is compared with the existing Tikhonov regularization [24, 27] and $\ell_1$-norm regularization [7, 25, 29], respectively. The parameters of different image reconstruction methods are listed in Table 3, and the reconstructed images are shown in Fig. 10 for the outdoor scenarios and Fig. 11 for the indoor scenarios.

**Table 3.** Image regularization reconstruction parameters.

| Parameter | Value | Description |
|---|---|---|
| $\mu_1$ | 30 | Tikhonov regularization [24, 27] |
| $\mu_2$ | 2.2 | $\ell_p$-norm regularization |
| $\mu_3$ | 20 | $\ell_1$-norm regularization [7, 25, 29] |
| $p$ | 0.4 | Selection of norm $p$ value |

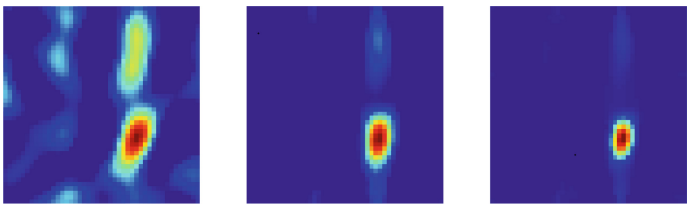

(a) Tikhonov (b) Tikhonov-$\ell_1$ (c) Tikhonov-$\ell_p$

**Fig. 10.** Reconstruction results of position 1 in outdoor scenarios.

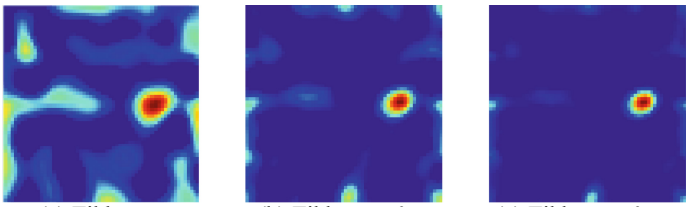

(a) Tikhonov (b) Tikhonov-$\ell_1$ (c) Tikhonov-$\ell_p$

**Fig. 11.** Reconstruction results of position 4 in indoor scenarios.

Compared with Tikhonov regularization as Fig. 10(a) and Fig. 11(a), the Tikhonov-$\ell_1$-norm and Tikhonov-$\ell_p$-norm regularization can further reduce the artifacts in reconstructed image, mainly because of consideration the sparsity of the attenuated image, thereby the smaller attenuation components from noise and multipath interference will be suppressed in sparse reconstruction; for $0 < p < 1$, Tikhonov-$\ell_p$-norm has the stronger ability of sparse reconstruction, resulting in the higher energy concentration and the less residual artifacts in the reconstructed images as Fig. 10(c) and Fig. 11(c). The corresponding imaging quality and positioning accuracy are shown in Table 4, and Fig. 12 for different target positions. From Table 4, the proposed RTI system can improve the average positioning accuracy ($RMSE_{(loc)}$) by 10.2% (compared to Tikhonov) and 5.0% (compared to Tikhonov-$\ell_1$-norm); and the imaging error can reduce by 48.0% (compared to Tikhonov) and 19.1% (compared to Tikhonov-$\ell_1$-norm). For different targets positions, the proposed Tikhonov-$\ell_p$-norm regularization can also show its superiority over the existing reconstruction methods as Fig. 12.

**Table 4.** RMSE of different reconstruction methods.

| | | Tikhonov | Tikhonov-$\ell_1$ | Tikhonov-$\ell_p$ |
|---|---|---|---|---|
| Imaging Quality | $RMSE_{(img)}$ | 0.2676 | 0.1720 | 0.1391 |
| | Median | 0.2418 | 0.1609 | 0.1311 |
| | Standard Deviation | 0.0291 | 0.0228 | 0.0303 |
| Positioning Accuracy (m) | $RMSE_{(loc)}$ | 0.1613 | 0.1526 | 0.1449 |
| | Median | 0.1458 | 0.1360 | 0.1323 |
| | Standard Deviation | 0.0264 | 0.0131 | 0.0179 |

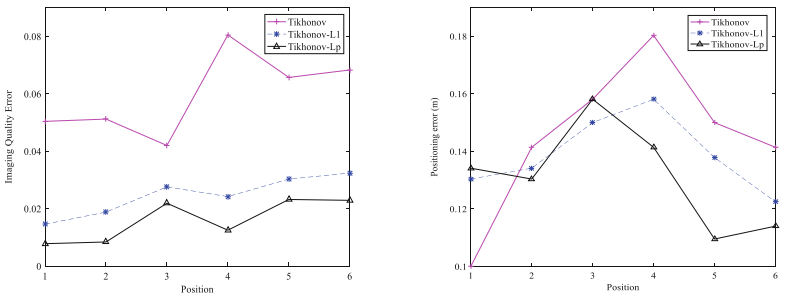


(a) Imaging quality (b) Positioning error

**Fig. 12.** RTI performance curves of different reconstruction methods.

## 5 Conclusions

This study describes one new imaging model in RTI system, which mainly involves the following works: 1) the horizontal distance attenuation factor is firstly introduced to the adaptive elliptical model for computing the voxel contribution in monitoring area with higher sensitiveness on shadowing effects, 2) considering the sparsity, Tikhonov-$\ell_p$-

norm-based image reconstruction ($0 < p < 1$) is combined into the imaging model, when the value of parameter $p$ is smaller than 1, the regularization parameter $\mu_2$ is far less than the existing Tikhonov regularization and $\ell_1$-norm regularization, which will make the reconstructed image more sparse, thereby the proposed imaging model can provide the higher energy concentration of the target position and the less artifacts in reconstructed image. It should be noted that the optimal parameter $p$ can only be decided by experiments in the proposed Tikhonov-$\ell_p$-norm-based image reconstruction.

**Author Contributions.** Chunhua Zhu and Zhen Shi proposed the original idea and Qinwen Ji carried out the experiment. Chunhua Zhu and Zhen Shi wrote the paper. Zhen Shi supervised and reviewed the manuscript. All authors read and approved the final manuscript.

**Funding.** This research was financially supported by National Science Foundation of China (61871176): Research of Abnormal Grain Conditions Detection using Radio Tomographic Imaging based on Channel State Information; National Science Foundation of China (61901159): Research on Beamspace Channel Estimation in Massive MIMO Systems by Fusing Multi-Dimensional Characteristic Information; Applied research plan of key scientific research projects in Henan colleges and Universities (19A510011); Research of Abnormal Grain Conditions Detection Based on Radio Tomographic Imaging based on RSSI; Scientific Research Foundation Natural Science Project In Henan University of Technology (2018RCJH18): Research of Abnormal Grain Conditions Detection using Radio Tomographic Imaging based on Received Signal Strength Information; the Innovative Funds Plan of Henan University of Technology Plan (2020ZKCJ02): Data-Driven Intelligent Monitoring and Traceability Technique for Grain Reserves.

**Conflicts of Interest.** The authors declare no conflict of interest.

## References

1. Wilson, J., Patwari, N.: Radio tomographic imaging with wireless networks. IEEE Trans. Mob. Comput. **9**(5), 621–632 (2010)
2. Wilson, J., Patwari, N.: Through walls: motion tracking using variance–based radio tomography networks. IEEE Trans. Mob. Comput. **10**(5), 612–621 (2011)
3. Hamilton, B.R., Ma, X., Baxley, R.J., Matechik, S.M.: Propagation modeling for radio frequency tomography in wireless networks. IEEE J. Sel. Top. Sig. Process. **8**(1), 55–65 (2014)
4. Tian, X., An, J., Wang, Z.: A const-eccentricity elliptical model in radio tomography imaging. J. Beijing Univ. Technol. **35**(07), 725–729 (2015)
5. Lei, Q., Zhang, H., Sun, H., Tang, L.: A new elliptical model for device-free localization. Sensors **16**(4), 1–12 (2016)
6. Zhu, C., Wang, J., Chen, Y.: ARTI (Adaptive Radio Tomographic Imaging): one new adaptive elliptical weighting model combining with tracking estimates. Sensors **19**(5), 1–12 (2019)
7. Xu, S., Liu, H., Gao, F., Wang, Z.: Compressive sensing based radio tomographic imaging with spatial diversity. Sensors **19**(3), 1–15 (2019)

8. Wang, M., Wang, Z., Bu, X., Ding, E.: An adaptive weighting algorithm for accurate radio tomographic image in the environment with multipath and WiFi interference. Int. J. Distrib. Sens. Netw. **13**(1), 1–11 (2017)
9. Zhu, C., Chen, Y.: Distance attenuation-based elliptical weighting model in radio tomography imaging. IEEE Access **6**, 34691–34695 (2018)
10. Ke, W., Zuo, H., Chen, M., Wang, Y.: Enhanced radio tomographic imaging method for device-free localization using a gradual-changing weight model. Progr. Electromagn. Res. M **82**, 39–48 (2019)
11. Kaltiokallio, O., Jantti, R., Patwari, N.: ARTI: an adaptive radio tomographic imaging system. IEEE Trans. Veh. Technol. **66**(8), 7302–7316 (2017)
12. Wang, J., Gao, Q., Pan, M., Zhang, X., Yu, Y., Wang, H.: Toward accurate device-free wireless localization with a saddle surface model. IEEE Trans. Veh. Technol. **65**(8), 6665–6677 (2016)
13. Wang, Z., Liu, H., Xu, S., Bu, X., An, J.: A diffraction measurement model and particle filter tracking method for RSS-based DFL. IEEE J. Sel. Areas Commun. **33**(11), 2391–2403 (2015)
14. Savazzi, S., Nicoli, M., Carminati, F., Riva, M.: A Bayesian approach to device-free localization: Modeling and experimental assessment. IEEE J. Sel. Top. Sig. Process. **8**(1), 16–29 (2014)
15. Wang, Z., Qin, L., Guo, X., Wang, G.: Dual-radio tomographic imaging with shadowing-measurement awareness. IEEE Trans. Instrum. Meas. **69**(7), 4453–4464 (2020)
16. Wang, J., et al.: E-HIPA: an energy-efficient framework for high-precision multi-target-adaptive device-free localization. IEEE Trans. Mob. Comput. **16**(3), 716–729 (2017)
17. Huang, K., Tan, S., Luo, Y., Guo, X., Wang, G.: Enhanced radio tomographic imaging with heterogeneous Bayesian compressive sensing. Pervasive Mob. Comput. **40**, 450–463 (2017)
18. Kaltiokallio, O., Bocca, M., Patwari, N.: Enhancing the accuracy of radio tomographic imaging using channel diversity. In: 2012 IEEE 9th International Conference on Mobile Ad-Hoc and Sensor Systems (MASS 2012), pp. 254–262. IEEE, Las Vegas (2012)
19. Bocca, M., Luong, A., Patwari, N., Schmid, T.: Dial it in: rotating RF sensors to enhance radio tomography. In: 2014 Eleventh Annual IEEE International Conference on Sensing, Communication, and Networking (SECON), pp. 600–608. IEEE, Singapore (2014)
20. Chartrand, R., Yin, W.: Iteratively reweighted algorithms for compressive sensing. In: 2008 IEEE International Conference on Acoustics, Speech and Signal Processing, pp. 3869–3872. IEEE, Las Vegas (2008)
21. Li, Z., Tang, J.: Unsupervised feature selection via nonnegative spectral analysis and redundancy control. IEEE Trans. Image Process. **24**(12), 5343–5355 (2015)
22. Chen, G., Chen, S.: Regularization method with $\ell$p-norm sparsity constraints for potential field data reconstruction. J. ZheJiang Univ. (Eng. Sci.) **48**(4), 748–756 (2014)
23. Zhang, T., Wu, H., Liu, Y., Peng, L., Yang, C., Peng, Z.: Infrared small target detection based on non-convex optimization with Lp-norm constraint. Remote Sens. **11**(5), 559 (2019)
24. Vogel, C.R.: Computational Methods for Inverse Problems. SIAM (2002)
25. Kanso, M.A., Rabbat, M.G.: Compressed RF tomography for wireless sensor networks: centralized and decentralized approaches. In: Krishnamachari, B., Suri, S., Heinzelman, W., Mitra, U. (eds.) DCOSS 2009. LNCS, vol. 5516, pp. 173–186. Springer, Heidelberg (2009). https://doi.org/10.1007/978-3-642-02085-8_13
26. Ma, M., Li, M., He, X., Liu, Y., Chen, X.: Research on ECT image reconstruction algorithm based on compression sensing and adaptive Lp norm. J. Mach. Tool Hydraulic Pressure **46**(12), 25–31 (2018)

27. Alippi, C., Bocca, M., Boracchi, G., Patwari, N., Rover, M.: RTI goes wild: radio tomographic imaging for outdoor people detection and localization. IEEE Trans. Mob. Comput. **15**(10), 2585–2598 (2015)
28. Denis, S., Berkvens, R., Ergeerts, G., Weyn, M.: Multi-frequency sub-1 GHz radio tomographic imaging in a complex indoor environment. In: 2017 International Conference on Indoor Positioning and Indoor Navigation (IPIN), pp. 1–8. IEEE, Sapporo, Japan (2017)
29. Cao, Z., Wang, Z., Fei, H., Guo, X., Wang, G.: Generative model based attenuation image recovery for device-free localization with radio tomographic imaging. Pervasive Mob. Comput. **66**, 1–13 (2020)
30. Ding, X., Choi, T. M., Tian, Y.: HRI: Hierarchic radio imaging-based device-free localization. IEEE Trans. Syst. Man Cybern. Syst. 1–14 (2020)